

MULTI-SCALE SIMULATION OF TWO-PHASE FLOWS IN ENERGY SYSTEMS

Bulat P. and Volkov K.*

*Author for correspondence

Faculty of Science, Engineering and Computing,
Kingston University,
London, SW15 3DW,
United Kingdom,
E-mail: k.volkov@kingston.ac.uk

ABSTRACT

A numerical analysis of the internal flows is performed to improve the current understanding and modelling capabilities of the complex flow characteristics encountered in energy systems. Simulation is divided into two stages, micro- and macro-scales. The averaged Navier–Stokes equations are solved numerically for the gas phase. The particulate phase is simulated through a Lagrangian deterministic and stochastic tracking models to provide particle trajectories. The particles are assumed to interact with a succession of turbulence eddies, as they move through the computational domain. The results obtained highlight the crucial significance of the particle dispersion in turbulent flow and high potential of statistical methods. Strong coupling between acoustic oscillations, vortical motion, turbulent fluctuations and particle dynamics is observed. Acoustic oscillations provide additional mechanism to transfer energy from periodic motions to turbulence leading to an enhanced level of turbulence intensity. Acoustic waves give rise to an early transition from laminar to turbulent flow through energy transfer from the organized oscillatory field to the broadband turbulent flowfield.

INTRODUCTION

Aluminum particles in solid propellants serve two purposes: increasing specific impulse and suppressing high-frequency combustion instability. Unlike the other ingredients, aluminum particles burn in a significant portion of the combustion chamber of solid rocket motor (SRM) and produce alumina smoke and agglomerates that are carried out into the flowfield [1]. The presence of aluminum droplets in the flowfield contributes to the motor performance loss through decreasing nozzle efficiency and surface damage from droplet impingement. Detailed knowledge of particulate phase characteristics as residue size, burning time and heat release as well as particle dynamics and particle dispersion in a turbulent flowfield are essential to improve motor performance and reliability. An analysis is hampered by the complex flow features involving complex geometry, turbulence with mass injection, recirculation regions, a wide range of Mach numbers, two-phase flow phenomena, heterogeneous combustion, and uncertainties in particle density and particle size distribution.

tion.

Turbulence plays an important role in determining the wave properties through the damping effect of turbulence-induced eddy viscosity on vortical motion. Turbulence modelling becomes necessary for the evaluation of heat transfer and related phenomena (e.g. erosive burning). The interactions between organized oscillatory motions and turbulent fluctuations give rise to additional mechanisms of energy production, transfer and dissipation of wave modes. The difficulty in simulation of turbulence comes from the fact the transition is always inside the SRM, since the velocity at the head-end is equal to zero.

Aluminum droplet combustion and alumina residue behavior in the combustion chamber of SRM affect combustion instabilities by acting as driving or damping mechanisms [2]. Some of aluminum droplets remain in the motor during its operation and collect in the aft-end region. Inside the motor, these droplets are the source of slag material. Alumina slag deposition at motor aft-end results in motor performance loss, damage of thermal protection due to overheating, and possible sloshing and ejection of liquid agglomerates through the nozzle, which may cause pressure disturbances and trust imbalance.

SRMs are subject to pressure oscillations caused by vortex shedding and acoustic feedback resulting from impingement of the vortices on the nozzle and other obstacles [3–5]. The oscillatory flowfield in a SRM consists of three distinct types of wave motions: acoustic (irrotational and compressible), vortical (rotational and incompressible) and entropy (arising from unsteady heat release) modes [6]. The coupling between the acoustic wave and the incoming radial mass flow from the propellant surface generates fluctuating vorticity and causes the energy transfer from the acoustic to the vortical field (flow-turning energy losses) [3,4]. The interactions between entropy fluctuations and non-uniform flow act as a strong source term for driving acoustic oscillations in regions with large velocity gradients [3,7]. The three waves, along with the transient combustion response of propellant, dictate the stability behavior of SRM.

Flow oscillations are expected to interact with the agglomeration process on the burning surface (mechanism 1), with the ignition and the distributed combustion that may occur in a

significant portion of the combustion chamber (mechanism 2) and with alumina residues in the entire volume of the chamber (mechanism 3). The first and the third interactions are identified as damping phenomena while the second is suspected to be a driving mechanism [2]. Their effectiveness depends on oscillation frequencies, droplet sizes and burning-to-residence time ratio [8]. Net contribution of aluminum to the global acoustic balance may be positive or negative [2, 3, 5].

At high frequencies, particles usually exert a damping effect on acoustic oscillations [2], and suppression of oscillations occurs due to the influence of agglomerates on the fluctuations on the burning surface (mechanism 1). At frequencies below 2000 Hz, mechanism 1 plays a minor role as compared to mechanism 3, but this interaction also leads to damping of oscillations. Some propellants that ensure stable combustion without metallic particles display a tendency to combustion instability due to addition of aluminum, which is caused by the influence of mechanism 2, which leads to enhancement of oscillations [9].

In order to extend the reliability of calculations as a predicting tool to be used for industrial applications in design and development of SRMs, one needs to improve the level of accuracy of physical models and the effectiveness of numerical schemes [10]. The study focuses on the development of numerical analysis of the internal two-phase flows with emphasis on the momentum and energy transfer between the gas and particles in presence of forced pressure oscillations, particle dynamics and particle dispersion in turbulent flowfield, interaction between turbulent and forced oscillatory flowfields, and effects of particles on steady and unsteady flow motions. In contrary to analysis performed in [11], particle motion and scattering in the channel with one side injection is studied.

MATHEMATICAL MODEL

The mathematical formulation of the problem is divided into micro- and macro-level models. Micro-level models correspond to the processes in the volume occupied by an individual particle. The high-level model corresponds to the processes in the volume occupied by multi-phase mixture. The data obtained from solution of micro-level problem (drag and lift coefficients, burning time) are used to calculate source terms in the governing equations describing macro-level problem.

The two-phase flow is simulated with combined Eulerian–Lagrangian approach. The unsteady Reynolds-averaged Navier–Stokes equations (RANS) are solved numerically for the gas phase. The particulate phase is simulated through a Lagrangian stochastic tracking model [12].

The governing equations of gas represent the conservation equations of mass, momentum and energy in Cartesian coordinates. The x axis is aligned with the centreline of the channel, and the y axis is aligned with the radius. The injection velocity, v_w , is assumed to be identical at all points of the propellant surface and to be directed normal to this surface. The parameters of the gas and particles entering the channel are assumed to be constant along the burning surface. Aluminum particles are injected from the surface of the channel at points uniformly distributed

over the channel length.

In Cartesian coordinates (x, y, z) , an unsteady 3D flow is described by the following equations (for simplicity, chemical reactions are not included)

$$\frac{\partial \rho}{\partial t} + \nabla \cdot (\rho v) = 0$$

$$\frac{\partial \rho v}{\partial t} + \nabla \cdot (\rho v v) = -\nabla p + \nabla \cdot \tau - F_p n_p$$

$$\frac{\partial \rho e}{\partial t} + \nabla \cdot [(\rho e + p)v] = -\nabla \cdot q + \nabla \cdot (\tau \cdot v) - W_p n_p - Q_p n_p$$

The pressure is found from the expression

$$p = (\gamma - 1)\rho \left[e - \frac{1}{2}(v_x^2 + v_y^2 + v_z^2) \right]$$

Here, t is the time, ρ is the density, v_x , v_y , and v_z are the velocity components in the coordinate directions x , y and z , p is the pressure, e is the total energy per unit mass, T is the temperature, and γ is the specific heat capacity ratio. The subscript p corresponds to the particles.

The viscous stress tensor and the heat flux vector are related to the velocity and temperature fields by the relations

$$\tau = \mu_e [\nabla v + (\nabla v)^*], \quad q = -\lambda_e \nabla T$$

where μ_e is the effective viscosity and λ_e is the effective thermal conductivity. The adjoint tensor is indicated by the asterisk. The effective viscosity, μ_e , is calculated as the sum of molecular viscosity, μ , and turbulent eddy viscosity, μ_t , and the effective thermal conductivity, λ_e , is expressed in terms of effective viscosity and Prandtl number

$$\mu_e = \mu + \mu_t, \quad \lambda_e = c_p \left(\frac{\mu}{Pr} + \frac{\mu_t}{Pr_t} \right)$$

where c_p is the specific heat capacity at constant pressure, and $Pr = 0.72$ and $Pr_t = 0.9$. The eddy viscosity is calculated by the Kolmogorov–Prandtl relationship ($\mu_t = c_\mu \rho k^2 / \varepsilon$).

The transport equations of the turbulent kinetic energy, k , and its dissipation rate, ε , are written in the form

$$\frac{\partial \rho k}{\partial t} + (\rho v \cdot \nabla) k = \nabla \cdot \left[\left(\mu + \frac{\mu_t}{\sigma_k} \right) \nabla k \right] + P - \rho \varepsilon + E_p$$

$$\frac{\partial \rho \varepsilon}{\partial t} + (\rho v \cdot \nabla) \varepsilon = \nabla \cdot \left[\left(\mu + \frac{\mu_t}{\sigma_\varepsilon} \right) \nabla \varepsilon \right] + \frac{\varepsilon}{k} (c_{\varepsilon 1} P - c_{\varepsilon 2} \rho \varepsilon) + \Phi_p$$

Here, P is the turbulent generation term.

The intensities of momentum and energy exchange between the phases are determined as the product of the number concentration of the particles and the intensity of interphase exchange per one particle. The work done by the particles on gas is calculated as $W_p = F_p \cdot v_p$. The source terms E_p and Φ_p in the equations of k - ϵ model take into account the effect of particulate phase on turbulence (turbulence modulation).

It is assumed that flow unsteadiness caused by external pressure oscillations exerts a minor effect on the flow core [13, 14]. The model constants are assigned the following values: $c_\mu = 0.09$, $\sigma_k = 1.0$, $\sigma_\epsilon = 1.3$, $c_{\epsilon 1} = 1.44$, $c_{\epsilon 2} = 1.92$.

The modified k - ϵ model demonstrates reasonable results for injection-driven flows in comparison with the experimental data and results from large-eddy simulation [2, 10, 12].

The particles are simulated through a Lagrangian deterministic or stochastic tracking models to provide particle trajectories [12]. The virtual mass and Basset forces due to their small magnitudes, and the Magnus force due to lack of knowledge about particle angular momentum are neglected. The resulting force acting on a particle is the drag force. The equations describing translational motion and convective heat transfer of a spherical particle in a turbulent flowfield are written in the form

$$\begin{aligned} \frac{dr_p}{dt} &= v_p \\ \frac{dv_p}{dt} &= \frac{3C_{Dp}}{8\rho_p r_p} |v - v_p| (v - v_p) \\ c_p^m m_p \frac{dT_p}{dt} &= 2\pi r_p \text{Nu}_p \lambda (T - T_p) \end{aligned}$$

To calculate the drag coefficient and the Nusselt number, solution of micro-level problem is used [1].

The fluid velocity represents a random function of the Cartesian coordinates and time. The fluid velocity is a sum of the averaged velocity, $\langle v \rangle$, and the random velocity, v' . The averaged velocity is found from the solution of RANS equations. The turbulence is taken into account by introducing random velocity fluctuations. The particles are assumed to interact with a succession of turbulence eddies, as they move through the computational domain [12]. The duration of interaction between an eddy and a particle is determined as the smaller one between the eddy life-time and the transit time required for a particle to transverse the eddy.

Equations for particles are integrated along the path of an individual particle and require specification of the initial conditions — the Cartesian coordinates, velocity, temperature and mass of a particle at the time $t = 0$ (on the injection surface).

NUMERICAL METHOD

Flow solution is provided using cell-centered finite volume formulation of unsteady 3D compressible RANS equations on unstructured meshes. Governing equations are solved by the fifth order Runge–Kutta time marching scheme. Piecewise parabolic

method (PPM) is applied to inviscid fluxes, and central difference scheme of the second order is applied to viscous fluxes. For the injection-driven flows, the fluid velocity in the bulk of the computational domain is much smaller than the acoustic speed. The conventional numerical algorithms developed for compressible flows encounter disparity of eigenvalues of the Jacobian and singular behavior of the pressure gradient in the momentum equation. Block-Jacobi preconditioning technique and dual time-stepping integration scheme are employed to stabilize calculations. The numerical scheme is efficient and robust over a wide range of Mach numbers.

To solve the Cauchy problem for particle equations, the fourth-order Runge–Kutta method and methods that permit resolving in the solution rapidly and slowly decaying components are used. To supply fluid parameters at points lying in the particle trajectory, the bi-linear interpolation method is employed. The integration time step along each trajectory is limited to the time and space turbulence scales. In the calculations, from 10^3 to 10^5 trajectories of sample particles depending on their size are modelled.

The unsteady calculations are performed in the following manner. After convergence toward a steady state solution, the channel flow is excited close to its first longitudinal mode by means of one period of head-end forcing. Pressure oscillations equal to 5% of the head-end mean pressure at imposed acoustic frequencies are forced at the head-end in order to analyze unsteady flowfield. Then, the response of the flowfield to that perturbations is analyzed in terms of frequency and exponential damping.

GEOMETRY AND MESH

The physical model consists of axisymmetric channel with a closed head-end. Length of channel is $L = 1.88$ m, and its radius is $h = 0.2$ m. The pre-mixed gas and aluminum particles are uniformly injected from the channel walls to simulate the evolution of combustion products of solid propellant.

The air flow rate is 20 kg/(m·s) that corresponds to the propellant burning rate of 10 mm/s and density of 2296 kg/m³. The Mach numbers based on the surface injection velocity is about 0.002. Periodic pressure oscillations with an amplitude of 5% of the mean pressure are imposed at the channel head-end to generate longitudinal standing acoustic waves in the computational domain. On the injection wall ($r = h$), the velocities of the gas and particulate phase are subjected to the normal injection conditions ($u = u_p = 0$, $v = v_p = -\phi v_w$, where ϕ takes into account initial dynamic non-equilibrium of the phases, $\phi = 0.01$). No-slip and no-penetration boundary conditions are applied to the solid wall. The temperature of the wall is fixed. Non-reflecting boundary conditions are applied to the channel outlet to allow for travelling acoustic waves in the channel.

A limited number of injection points located on the channel surface are considered. The particles are distributed following a uniform law. Three different particle diameters are considered (10, 20 and 100 μm).

The computational mesh consists of 400 nodes in the axial

direction, and 100 nodes in the radial direction. The mesh nodes are clustered near the injection surface to resolve the vortical wave structure and turbulent boundary layer. The smallest mesh step size near the channel walls corresponds to $y^+ \sim 5$, and each vortical wavelength is covered by 10 nodes. Mesh sensitivity analysis is performed using meshes with a different number of nodes in Cartesian directions.

RESULTS AND DISCUSSION

In the unsteady case, the flow structure near the wall is complicated and testifies to the presence of an acoustic boundary layer inside which there are velocity fluctuations induced by propagation of unsteady shear waves (vorticity waves) [3, 5]. Vorticity perturbations are formed due to injection from the surface owing to the no-slip conditions on the wall, propagate inward the channel, and are damped by viscous effects. In the flow core, there is 1D distribution of the axial velocity fluctuations, which is accurately described by the existing linear theory [3]. The influence of viscosity on propagation of vorticity waves is proportional to the frequency of oscillations. Flow turbulence leads to more appreciable damping of the amplitude of the axial velocity fluctuations because of additional generation of eddy viscosity.

The overall flow development is described by three distinct regimes as shown in the Figure 1: laminar (region 1), transitional (region 2) and turbulent (region 3). Viscous effects play an important role in the vicinity of the head-end ($0 < x/h < 1/Re$). The flow is predominantly laminar in the upstream part of the channel ($0 < x/h < 5$) and undergoes transitions to turbulence as a result of hydrodynamic instability ($5 < x/h < 10$). Unlike channel flow with solid walls, the outbreak of turbulence occurs away from the walls (shaded region). The peak of turbulence intensity moves closer to the wall in the downstream direction until the surface injection prohibits further penetration of turbulence ($10 < x/h < 60$). As the flow develops farther downstream, the profile of axial velocity becomes much steeper near the wall, but flatter in the core region (near the centreline).

Profiles of axial velocity predicted with the developed model (solid lines) more flatter in the core region and more steeper in the near wall region than those in vortical flow (dashed lines). The profiles of radial velocity predicted with RANS and model of vortical flow are in a good agreement. Compressibility effects in the downstream part of the channel lead to small discrepancy of the results based on different models. Reynolds number has a small influence on profiles of axial and radial velocities in channel formed by wall injection.

A negative pressure gradient due to flow acceleration exists in the injection-driven flow, which exerts an appreciable effect on the mechanism and intensity of turbulent transfer. Laminar to turbulent transition occurs further downstream (except for the near-wall and near-centreline regions), which is manifested in the presence of a turbulence front and displacement of the turbulent kinetic energy peak from the wall inward the flow. Near the channel wall, there is a layer with a low (tending to zero) of the turbulent kinetic energy (displacement zone). Near the injec-

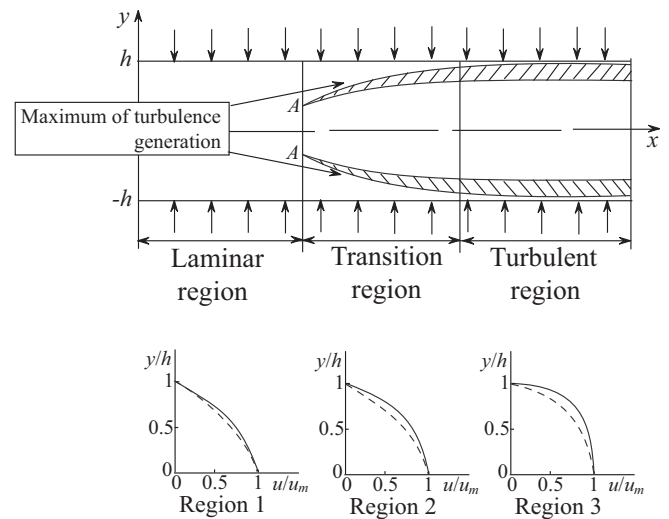


Figure 1. Flow regimes in channel with fluid injection

tion wall and the channel centreline, the flow is virtually laminar. An increase in the level of turbulent velocity oscillations is observed in the strong shear region at a certain distance from the channel wall, where the fluid particles moving normal to the surface change the direction of their motion to the opposite one in a narrow subsurface layer.

The profiles of the longitudinal velocity and turbulent kinetic energy over the channel cross-section are presented in the Figure 2 for different injection velocities from the upper wall of the channel. The symbols \bullet present the data of the physical experiment, and symbols \circ present the results of the calculation with the original k - ϵ turbulence model at $v_w = 1$ m/s (conditions for line 3). The dashed line corresponds to the cosine longitudinal velocity profile taking place in a vortex flow of inviscid incompressible fluid, and the dotted dashed line shows the velocity profile of a laminar flow of a viscous incompressible fluid at $Re = 10^3$. As the Reynolds number increases, the maximum of the longitudinal velocity component approaches the impermeable surface, near which a viscous flow zone similar to the boundary layer on a flat plate develops.

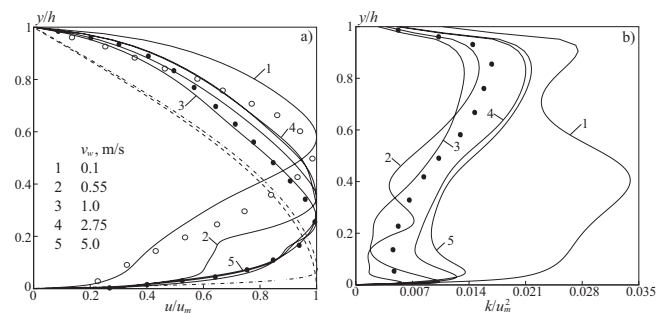


Figure 2. Profiles of the longitudinal velocity (a) and turbulent kinetic energy (b) over the channel cross-section at $x/h = 30$

Acoustic oscillations exert significant influence on unsteady flow evolution. In particular, single-harmonic oscillations excite a fluctuating flow with a broadband frequency spectrum [3]

(this phenomenon is referred to as acoustically induced turbulent motion). Generation of turbulence by organized external forcing is viewed as an energy transfer process from the acoustic flowfield to the turbulent flowfield. The coupling between the Reynolds stresses and the gradient of acoustic velocity provides a mechanism to transfer the kinetic energy from acoustic motions to turbulent fluctuations. Furthermore, an early transition from laminar regime to turbulent one occurs depending on the forcing amplitude and frequency (Figure 1). The effect of energy exchange tends to be more profound for low-frequency acoustic oscillations.

The radial profiles of time-averaged axial velocity and turbulent kinetic energy at various axial locations (solid lines) are shown in the Figure 3 and Figure 4 for the first longitudinal mode ($f \sim 1000$ Hz, $\phi = 0.02$). Lines 1 correspond to the simulation of the injection-driven flow based on RANS equations and $k-\epsilon$ model, and lines 2 correspond to large-eddy simulation of channel flow induced by wall injection. The profiles corresponding to steady state flow (dashed lines) are also included for comparison. An enhanced level of turbulence due to acoustic excitation is clearly observed. The acoustic waves induce flow instability and cause transfer of energy from the oscillatory organized to the turbulent field.

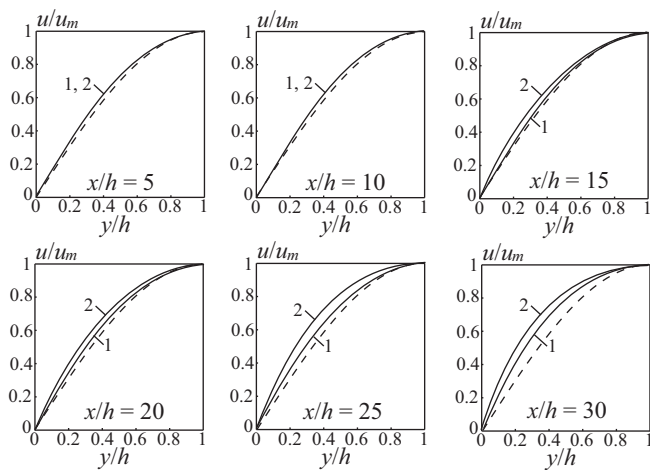


Figure 3. Radial profiles of axial velocity

As the ratio of the particle relaxation time to the acoustic time for fine particles is comparatively small ($Stk \rightarrow 0$), they respond to the turbulent oscillations of the carrier flow velocity and, therefore, to changes in its parameters and follow the acoustic velocity fluctuations. Coarse particles ($Stk \rightarrow \infty$) do not respond to the turbulent oscillations of the fluid flow velocity.

The results of calculation of the motion and scattering of aluminum oxide particles ($r_p = 5-10 \mu\text{m}$) for various particle sizes (Stokes numbers) are shown in the Figure 5. At the initial instant of time the particle was on the upper wall of the channel. The calculations were made beginning from the point $x_{p0} = 3$ with a step $\Delta x = 0$. The calculation was finished when the particle either left the calculated region (at $x/h > 30$) or fell onto the lower wall of the channel (at $y = 0$). The degree of involvement of a particle in pulsation motion is determined by the rela-

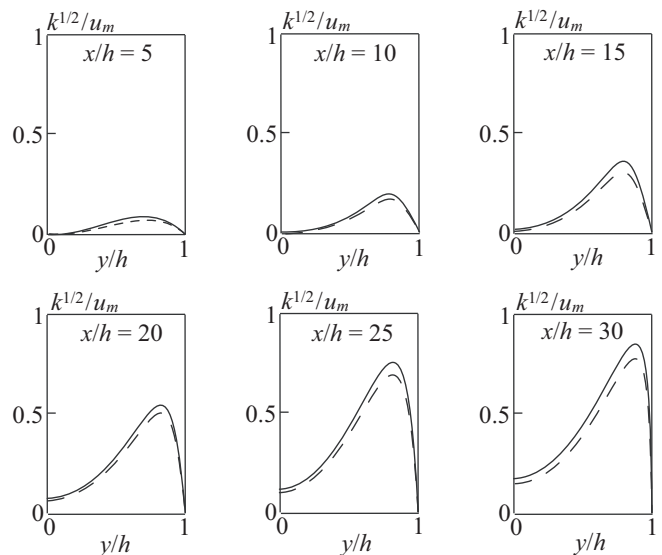


Figure 4. Radial profiles of turbulent kinetic energy

tion between the dynamic relaxation time of the particle and the characteristic time scale of turbulence. The inhomogeneity of the carrier phase turbulence field for particles of small fractions leads to the appearance of turbulent migration of the particle in the direction of decreasing pulsation energies of the gas.

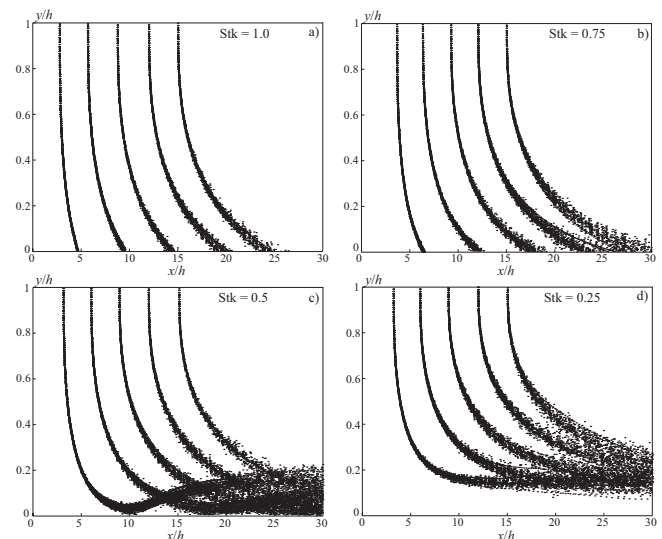


Figure 5. Trajectories of sample particles in the channel with one-side injection ($v_w = 5$ m/s)

For particles of large fractions ($r_p = 30-50 \mu\text{m}$), velocity fluctuations produce no significant effect on the impurity motion throughout the region of flow development because of the inertia of such particles. Weak migration of particles towards decreasing pulsation energies of the gas is observed only for particles injected into the channel at a considerable distance from its left end (at $x_{p0} > 9$). Small particles ($r_p = 5-15 \mu\text{m}$) are scattered rather strongly. The degree of scattering (dispersion of particle displacement) is the higher the smaller the particle size and the farther from the left boundary of the calculated region it is in-

jected into the channel (the kinetic turbulence energy and the rms velocity of the carrier flow vary along the x coordinate according to a law close to the parabolic one).

The oscillatory velocity field is split into acoustic and vortical flow motions. Several two-phase flow simulations are carried out to study the effects of the particle Stokes number on the oscillations behavior.

The Figure 6a shows the radial profiles of amplitude of axial velocity fluctuations ($f \sim 3770$ Hz, $\phi = 0.02$) at the mid-section of channel ($x/L \sim 0.5$) where flow is turbulent. The influence of large particles on the acoustic velocity is negligible because of their high inertia, and small particles effectively reduce the velocity oscillations. Turbulence exerts a small influence on the acoustic wave structure. Its primary contribution lies in the dissipation of the vortical motion through the turbulence-enhanced eddy viscosity. The Figure 6b shows results of the first longitudinal mode oscillations ($f \sim 943$ Hz, $\phi = 0.02$). The damping effect of particles on the vortical flow motion is observed. An optimum size of particles corresponding to acoustic Stokes number close to unity is obtained to exert the maximum dissipation on flow oscillations.

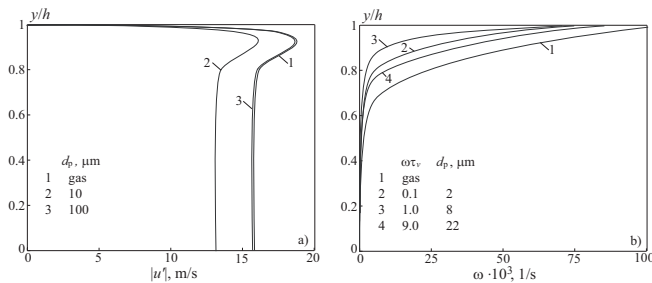


Figure 6. Effect of particles on acoustic and vortical flow fields at $m_p = 0.2$

Figure 7 shows the radial profiles of the amplitude of axial velocity fluctuations in a laminar flow at a point located approximately in the middle of the channel ($x/L = 0.5$) for $f = 1885$ Hz and $\phi = 0.02$. The flow is laminar, the mass fraction of particles is assumed to be $m_p = 0.2$, and the initial particle velocity is 0.1 m/s, which approximately corresponds to 10% of the injection velocity.

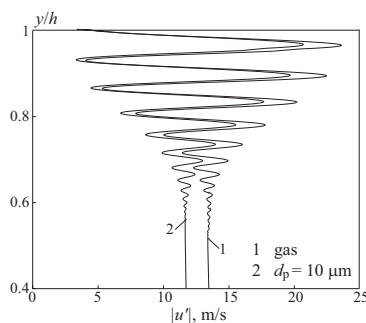


Figure 7. Radial profiles of the amplitude of axial velocity fluctuations

There are two characteristic flow regions. In the near-wall region of the flow ($y/h > 0.6$), there are significant oscillations of

acoustic velocity and vorticity. In the axial region ($y/h < 0.6$), the vorticity waves decay because of viscous dissipation, and the influence of acoustic effects starts to dominate. The presence of particles leads to suppression of acoustic velocity fluctuations owing to momentum and energy exchange with the gas. The overall effect of the particulate phase is determined by the particle loading, dynamic and thermal particle relaxation times, and frequency of acoustic oscillations. Fine particles exert a significant effect on the acoustic flowfield, rapidly reaching equilibrium with the gas and effectively changing the density of the mixture, whereas coarse particles exert a minor effect. The maximum amplitude of axial velocity fluctuations is $|u'|_{\text{max}} = 13.2$ m/s for $d_p = 10 \mu\text{m}$ and $|u'|_{\text{max}} = 15.5$ m/s for $d_p = 100 \mu\text{m}$ (this value coincides with the corresponding value in the pure gas).

CONCLUSION

Particle trajectories are computed to assess the effects of the turbulent flowfield on the slag dispersion for different particle diameters. Turbulent dispersion is mainly observed for small particles. Dispersion of particles leads to increasing particle residence time and changes combustion efficiency. The ratio of particle relaxation time to acoustic characteristics time plays an important role in dictating the two-phase flow interactions with oscillatory internal flow. A maximum attenuation of acoustic waves occurs when those times are comparable. Small particles exert greater influence on the dispersion of acoustic wave through its effective modification of mixture compressibility.

Acoustic oscillations provide additional mechanism to energy transfer from periodic motion to turbulence leading to an enhanced level of turbulence and an early transition from laminar to turbulence. On the other hand, eddy viscosity tends to suppress vortical flow motion caused by acoustic waves. Fine particles (equilibrium flow) exert the most pronounced damping effect at high frequencies of oscillations. For coarse particles, which are not involved into the wave motion (frozen flow), momentum and heat exchange with the gas is negligibly small, and the effect of particles on acoustic oscillations in the channel is not observed.

REFERENCES

- [1] Volkov, K.N., Combustion of single aluminium droplet in two-phase flow, *Heterogeneous Combustion*, Nova Science, 2011, pp. 191–260
- [2] Dupays, J., Two-phase unsteady flow in solid rocket motors. *Aerospace Science and Technology*, Vol. 6, No. 6, 2002, pp. 413–422
- [3] Flandro, G.A., Effects of vorticity on rocket combustion stability, *Journal of Propulsion and Power*, Vol. 11, No. 4, 1995, pp. 607–625
- [4] Vuillot, F., Vortex-shedding phenomena in solid rocket motors, *Journal of Propulsion and Power*, Vol. 11, No. 4, 1995, pp. 626–639
- [5] Apte, S.V., and Yang, V., Unsteady flow evolution and combustion dynamics of homogeneous solid propellant in a rocket motor, *Combustion and Flame*, Vol. 131, No. 1–2, 2002, pp. 110–131
- [6] Cai, W., Ma, F., and Yang, V., Two-phase vorticoacoustic flow

- interactions in solid-propellant rocket motors, *Journal of Propulsion and Power*, Vol. 19, No. 3, 2003, pp. 385–396
- [7] Culick, F.E.C., The stability of one-dimensional motions in a rocket motor, *Combustion Science and Technology*, Vol. 7, No. 4, 1973, pp. 165–175
- [8] Temkin, S., Attenuation and dispersion of sound in dilute suspensions of spherical particles, *Journal of Acoustical Society of America*, Vol. 108, No. 1, 2000, pp. 126–146
- [9] Brooks, K.P., and Beckstead, M.W., Dynamics of aluminum combustion, *Journal of Propulsion and Power*, Vol. 11, No. 4, 1995, pp. 769–780
- [10] Emelyanov, V.N., Teterina, I.V., and Volkov, K.N., Simulation of turbulent two-phase flows in the combustion chambers of solid rocket motors, *Proceedings of the 5th European Conference for Aeronautics and Space Sciences, 1–5 July 2013, Munich, Germany*, 2013, pp. 1–15
- [11] Emelyanov, V.N., and Volkov, K., Multi-scale simulation of turbulent two-phase flows induced by injection of fluid and particles, *Proceedings of the 7th European Combustion Meeting, 31 March - 1 April 2015, Budapest, Hungary*, 2015, 4249
- [12] Volkov, K., Internal turbulent two-phase flows formed by wall injection of fluid and particles, *Proceedings of the 5th ECCOMAS Computational Fluid Dynamics Conference, 14–17 June 2010, Lisbon, Portugal*, 2010, 01649
- [13] Cousteix, J., Desopper, A., and Houdeville, R., Structure and development of a turbulent boundary layer in an oscillating external flow, *Proceedings of the First International Symposium on Turbulent Shear Flows, 18–20 April 1977, Pennsylvania State University, Pennsylvania, USA*, 1977, pp. 154–171
- [14] Ramaprian, B.R., and Tu, S.W., An experimental study of oscillatory pipe flow at transitional Reynolds numbers, *Journal of Fluid Mechanics*, Vol. 100, No. 3, 1980, pp. 513–544